1 **Simulation of the effects of low volatility organic compounds on aerosol number**

2 **concentrations in Europe**

4 David Patoulias[1,2] and Spyros N. Pandis[1,2]

6 [1] Department of Chemical Engineering, University of Patras, Patras, Greece

7 [2] Institute of Chemical Engineering Sciences, Foundation for Research and Technology – Hellas

8 (FORTH/ICE-HT), Patras, Greece

10 **Abstract**

11 PMCAMx-UF, a three-dimensional chemical transport model focusing on the simulation of the

12 ultrafine particle size distribution and composition has been extended with the addition of reactions

13 of chemical aging of semi-volatile anthropogenic organic vapors, the emissions and chemical

14 aging by intermediate volatile organic compounds (IVOCs) and the production of extremely low

15 volatility organic compounds (ELVOCs) by monoterpenes. The model is applied in Europe to

16 quantify the effect of these processes on particle number concentrations. The model predictions

17 are evaluated against both ground measurements collected during the PEGASOS 2012 summer

18 campaign across many stations in Europe and airborne observations by a Zeppelin measuring

19 above Po-Valley, Italy. PMCAMx-UF reproduces the ground level daily average concentrations

20 of particles larger than 100 nm (N_{100}) with normalized mean error (NME) of 45% and normalized

21 mean bias (NMB) close to 10%. For the same simulation, PMCAMx-UF tends to overestimate the

22 concentration of particles larger than 10 nm (N_{10}) with a daily NMB of 23% and a daily NME of

23 63%. The model was able to reproduce more than 75% of the N_{10} and N_{100} airborne observations

24 (Zeppelin) within a factor of 2.

25   The ELVOC production by monoterpenes is predicted to lead to surprisingly small changes

26 of the average number concentrations over Europe. The total number concentration decreased due

27 to the ELVOC formation by 0.2%, the N_{10} decreases by 1.1%, while N_{50} increased by 3% and N_{100}

28 by 4% due to this new SOA source. This small change is due to the nonlinearity of the system with

29 increases predicted in some areas and decreases in others, but also the cancelation of the effects of

30 the various processes like accelerated growth and accelerated coagulation. Locally, the effects can

31 be significant. For example, an increase in N_{100} by 20-50% is predicted over Scandinavia and

32 significant increases (10-20%) over some parts of central Europe. The ELVOCs contributed on

33 average around 0.5 µg m^{-3} and accounted for 10-15% of the PM$_{2.5}$ OA. The addition of IVOC

34 emissions and their aging reactions led to surprising reduction of the total number of particles (N_{tot})

35 and N_{10} by 10-15 and 5-10%, respectively, and to an increase of the concentration of N_{100} by 5-

36 10%. These were due to the accelerated coagulation and reduced nucleation rates.

38 **1. Introduction**

39   Two major processes are responsible for the introduction of new particles in the

40 atmosphere: direct emission from numerous sources and nucleation from low-volatility vapors.

41 New particles formed by nucleation can either grow by condensation of vapors (e.g. sulfuric acid,

42 ammonia, nitric acid, and organics) to larger sizes becoming cloud condensation nuclei (CCN) and

43 thereby increasing the cloud droplet number concentration (CDNC) or affected by coagulation

44 with pre-existing larger particles and be lost (Adams and Seinfeld, 2002). Globally, according to

45 large-scale model simulations, atmospheric new particle formation (NPF) and subsequent particle

46 growth represent the most significant source of atmospheric aerosol particles, at least in terms of

47 their total number concentration (Kulmala et al., 2004; Makkonen et al., 2009; Merikanto et al.,

48 2009; Pierce and Adams, 2009; Wang and Penner, 2009; Yu and Luo, 2009). An increase of the

49 number concentration of particles that can act as CCN results in higher CDNC and brighter clouds

50 with longer lifetimes.

51   Globally, organic particulate matter makes up more than 50% of the sub-micrometer mass

52 concentration of ambient aerosols in locations throughout the world (Kanakidou et al., 2005;

53 Seinfeld and Pandis, 2006; Zhang et al., 2007). Nearly 70% of this material is thought to be

54 secondary organic aerosol (SOA) formed from the oxidation of volatile organic compounds

55 (VOCs) (Hallquist et al., 2009; Schulze et al., 2017). Many of the relevant precursor VOCs are

56 biogenic in origin, such as monoterpenes ($C_{10}H_{16}$) and isoprene (C_5H_8).

57   Several recent field studies have shown that SOA in polluted areas cannot be explained by

58 the simulation of only the first generation of reactions of "traditional" SOA precursors: biogenic

59 compounds (monoterpenes, sesquiterpenes, and isoprene) and anthropogenic compounds

60 (aromatics, olefins and large alkanes) (de Gouw et al., 2005; Volkamer et al., 2006; Kleinman et

61 al., 2008; Docherty et al., 2008; Matsui et al., 2009; Dzepina et al., 2009). At the same time, it has

become clear that organic vapors are responsible for most of the new particle growth in environments with low sulfur dioxide levels (Olenius et al., 2018; Yli-Juuti et al., 2020).

Traditional treatment of SOA formation considers only VOCs as the precursors and only semivolatile products (Odum et al., 1996). Robinson et al. (2007) suggested that intermediate volatile organic compounds (IVOCs) either emitted directly or resulting from the evaporation of particles may be an important and previously neglected pool of precursors for SOA formation. In addition, later generations of reactions of the products of VOCs, IVOCs and SVOCs can lead to products of even lower volatility and formation of SOA (Donahue et al., 2006). These chemical reactions can lead to continued SOA production after complete precursor consumption as products undergo further oxidation (Kroll et al, 2006; Ng et al., 2006).

Secondary extremely low volatile organic compounds (ELVOCs) have been detected both in the ambient atmosphere and laboratory studies (Donahue et al., 2011). These compounds promote new particle growth and CCN production in the atmosphere (Jokinen et al., 2015; Kirkby et al., 2016). ELVOCs can be produced rapidly in the gas phase during monoterpene oxidation (Ehn et al., 2014), and can enhance atmospheric new particle formation and growth (Jokinen et al., 2015). Due to their exceptionally low volatility, ELVOCs condense essentially irreversibly onto growing particles at a rate controlled by the Fuchs-adjusted particle surface area (Shrivastava et al., 2017).

Fanourgakis et al. (2019) evaluated 16 global chemistry transport models during a 4-year period and compared their prediction to the near-surface observed number concentration of aerosol particles across Europe and Japan. All models tended to underestimate the number concentrations for particles larger than 50 nm (N_{50}). The normalized mean bias (NMB) was −51% and normalized mean error (NME) was 55% for all stations. Sengupta et al. (2021) used the GLOMAP (Global Model of Aerosol Processes; Spracklen et al., 2005) modal aerosol microphysics model (Mann et al., 2010) simulating the production of six surrogate SOA species from the oxidation of anthropogenic VOCs, monoterpenes, and isoprene. They assumed that ELVOCs derive only from biogenic sources and can nucleate to form new particles (Gordon et al., 2016). Concentrations of particles larger than 3 nm (N_3) and particles larger than 50 nm (N_{50}) were consistently underestimated, while the best model performance was achieved when the ELVOC yield from precursor VOCs was around 13 %. These studies suggest that the role of organics and especially ELVOCs on particle formation and growth is still not well understood.

93   In this study we extend the three-dimensional regional chemical transport model (CTM),

94   PMCAMx-UF (Jung et al., 2010), with detailed aerosol microphysics (Gaydos et al., 2007; Karydis

95   et al., 2007) that has been used and evaluated for simulations over the US and Europe (Fountoukis

96   et al., 2012). Originally the model assumed that growth of new particles was exclusively due to

97   sulfuric acid and ammonia condensation while the semivolatile secondary organics condensed only

98   on the accumulation mode thus contributing to the condensation and coagulation sinks. This initial

99   model version was found to reproduce more than 70% of the hourly number concentrations of

100   particles larger than 10 nm (N_{10}) within a factor of 2 (Fountoukis et al., 2012). However, the

101   concentration of particles larger than 100 nm (N_{100}, a proxy for the number of particles that can act

102   as CCN) was systematically underpredicted. The growth rates were also underpredicted, with

103   smaller errors in sites where the sulfate to organics mass ratio was high. These problems were

104   caused mainly by insufficient organic vapor condensation (Fountoukis et al., 2012) on ultrafine

105   particles. Patoulias et al. (2018) developed an extended version of PMCAMx-UF in which the

106   SOA components were modeled as semi-volatile first-generation products of the oxidation of

107   VOCs. The model predictions were compared against size distribution measurements from 16

108   stations in Europe during a photochemically active period. Including SOA condensation on

109   ultrafines in PMCAMx-UF improved its ability to reproduce the N_{10} and N_{100} concentration at

110   ground level. The inclusion of SOA decreased the daily normalized mean bias (NMB) of N_{10} from

111   85% to 75% and the daily NMB of N_{100} from 40% to 20%. However, the results suggested that

112   there is a need for additional improvements.

113   The primary goal of this study is to examine the role of IVOCs and ELVOCs on particle

114   number concentrations in Europe. PMCAMx-UF is extended once more to simulate the multiple

115   generations of IVOC gas-phase oxidation and the production of ELVOCs by monoterpenes. The

116   model predictions are compared with measurements from 26 sites during the intensive field

117   campaign that took place in Europe, as part of the Pan-European-Gas-AeroSOl-climate-interaction

118   Study (PEGASOS) project, from June 5 to July 8, 2012. The airborne data obtained by a Zeppelin

119   measuring above Po-Valley during the same campaign are also used. An analysis of the Zeppelin

120   measurement can be found by Lampilahti et al. (2021).

121

122

123

2. Model description

124

125   PMCAMx-UF is a three-dimensional chemical transport model (CTM) that simulates the

126   aerosol number size distribution in addition to the mass/composition size distribution (Jung et al.,

127   2010; Fountoukis et al., 2012) and is described in detail in Patoulias et al. (2018). PMCAMx-UF

128   is based on the framework of PMCAMx (Gaydos et al., 2007; Karydis et al., 2007), describing the

129   processes of horizontal and vertical advection, emissions, horizontal and vertical dispersion, wet

130   and dry deposition, aqueous and aerosol phase chemistry, as well as aerosol dynamics and

131   thermodynamics.

132   For the simulation of aerosol microphysics, PMCAMx-UF uses the updated version of

133   DMANx which simulates the processes of coagulation, condensation/evaporation and nucleation

134   (Patoulias et al., 2015) with the two-moment aerosol sectional (TOMAS) algorithm (Adams and

135   Seinfeld, 2002; Jung et al., 2006). A key feature of TOMAS is its ability to track two independent

136   moments of the aerosol size distribution for each size bin: the aerosol number and mass

137   concentration.

138   The aerosol size distribution is discretized into 41 sections covering the diameter range from

139   approximately 0.8 nm to 10 μm. The lowest boundary is at 3.75×10^{-25} kg of dry aerosol mass per

140   particle. Each successive boundary has twice the mass of the previous one. The particle

141   components modeled include sulfate, ammonium, nitrate, sodium, chloride, crustal material,

142   water, elemental carbon, primary organic aerosol (POA) and eight surrogate SOA components.

143   In this work, the nucleation rate is calculated using a scaled ternary parameterization based

144   on the original expressions of Napari et al. (2002) with a scaling factor of 10^{-6} following the

145   suggestions of Fountoukis et al. (2012). The binary parameterization of Vehkamäki et al. (2002)

146   is employed if the NH_3 concentration is below a threshold value of 0.01 ppt.

147   Coagulation of particles in the atmosphere is an important sink of aerosol number but is

148   also a mechanism by which freshly nucleated particles grow to larger sizes. Following Adams and

149   Seinfeld (2002), TOMAS assumes that the aerosol particles coagulate via Brownian diffusion and

150   the effects of gravitational settling and turbulence are negligible. The calculation of the coagulation

151   coefficients is based on the wet diameters of the particles. These wet diameters are calculated

152   following the approach of Gaydos et al. (2005). For small particles (<100 nm), we use the

153   expression of Dahneke et al. (1983) to correct for non-continuum effects. The coagulation

154   algorithm uses an adaptive time step. The time step is limited so that the aerosol number or mass

155 concentration in any size category does not increase by more than an order of magnitude or
156 decrease by more than 25% in each step.

157   The extended SAPRC (Statewide Air Pollution Research Center) chemical mechanism
158 (Carter, 2000; Environ, 2003), which includes 219 reactions of 64 gases and 18 free radicals, is
159 used for the gas phase chemistry mechanism in PMCAMx-UF. The SAPRC version used for this
160 work includes five lumped alkanes (ALK1-5), two lumped olefins (OLE1-2), two lumped
161 aromatics (ARO1-2), isoprene (ISOP), a lumped monoterpene (TERP) and a lumped sesquiterpene
162 species (SESQ).

163

2.1   Secondary organic aerosol formation

165   Gas-phase oxidation of volatile organic compounds (VOCs) produces semi-volatile and
166 low-volatility products that can then condense to the particle phase. The volatility-basis set (VBS)
167 framework used in PMCAMx-UF (Donahue et al., 2006) describes the volatility distribution of
168 the OA compounds. SOA is formed from anthropogenic (aSOA) and biogenic (bSOA) precursors.
169 Each of these types is simulated with 5 volatility bins with saturation concentrations of 10^{-5}, 1, 10,
170 100 and 1000 µg m^{-3}. The 10^{-5} µg m^{-3} bin was added in this work to describe the ELVOCs. We
171 assumed an average molecular weight of 200 g mol^{-1} for SOA, and an effective enthalpy of
172 vaporization of 30 kJ mol^{-1} (Pathak et al., 2007; Stanier et al., 2007). The SOA yields used in this
173 version of PMCAMx-UF for the semi-volatile components are the NO_x-dependent stoichiometric
174 yields of Murphy at al. (2009).

175   Chemical reactions that change the volatility of the organics in the gas phase will change
176 the OA mass by influencing their partitioning. In PMCAMx-UF all secondary species are treated
177 as chemically reactive. Further gas-phase oxidation of OA vapors (chemical aging) is modeled
178 using a second-order reaction with hydroxyl radicals and a rate constant of 1×10^{-11} cm^3 molec^{-1} s^{-1}
179 (Atkinson and Arey, 2003). Each reaction is assumed to reduce the volatility of the vapor material
180 by one order of magnitude (i.e., shifting material from a C* of 100 to 10 µg m^{-3}), with a small
181 increase in mass (7.5%) to account for the added oxygen (Lane et al., 2008; Shrivastava et al.,
182 2008). Intermediate volatility organic compounds (IVOCs), are distributed in the 10^3, 10^4, 10^5, and
183 10^6 µg m^{-3} saturation concentration bins. The emission rates of the IVOCs are assumed to be equal
184 to 0.3, 0.4, 0.5 and 0.8 times the original non-volatile POA emission rate, for the 10^3-10^6 bins
185 respectively (Robinson et. 2007).

186   ELVOCs were assumed to be produced by the oxidation of monoterpenes with a molar

187   yield of 5%. For comparison, ELVOC yields for the α-pinene ozonolysis in Jokinen et al. (2015)

188   were 3.4 ± 1.7%, by Ehn et al. (2014) of 7 ± 4% and 4.5 ± 3.8% in Rissanen et al. (2014). An

189   average molecular weight of 200 g mol^{-1} for ELVOCs was assumed in this work.

190   The partitioning of OA between the gas and particulate phases is simulated dynamically in

191   PMCAMx-UF without assuming equilibrium (Patoulias et al., 2015). The driving force for

192   condensation of a vapor to an aerosol particle is the difference between its ambient vapor partial

193   pressure and the equilibrium vapor pressure over the particles, with the latter including the Kelvin

194   effect which is due to the curvature of the particles. The Kelvin effect is larger for the smaller

195   particles and acts as a barrier for the condensation of organic vapors on these particles. In this

196   simulation a surface tension of σ=0.025 Nm^{-1} is assumed for all SOA components (Pierce et al.,

197   2011; Patoulias et al. 2015).

198   Three different chemical aging schemes are used in this work (Table S1). The first scheme

199   (case 1 or base case) includes (i) the aging of SOA components from anthropogenic sources, using

200   a rate constant k (298 K) = $10×10^{-12}$ cm^3 molec^{-1} s^{-1} (anthropogenic SOA aging), (ii) the aging of

201   IVOCs using a rate constant k (298 K) = $40×10^{-12}$ cm^3 molec^{-1} s^{-1}, (iii) production of ELVOCs

202   with saturation concentration of 10^{-5} µg m^{-3} from the oxidation of monoterpenes with a yield of

203   5%. The aSOA aging rate constant is based on OH oxidation of the products of aromatic VOCs

204   oxidation (Atkinson 2000; 2003). No biogenic SOA aging was simulated in this case, an

205   assumption based on laboratory studies (Presto et al., 2006; Ng et al., 2006) and the results of Lane

206   et al. (2008). In the second simulation (case 2), the ELVOC yield was set to zero thus neglecting

207   their formation. The rest of the parameters were the same as in the base case. Finally, in the third

208   simulation the emissions of IVOCs and the chemical aging reactions of all VOCs were neglected

209   while the production of the ELVOCs was simulated similarly to the base case.

210

211   **2.2   Model application and measurements**

212   The PMCAMx-UF modeling domain in this application covers a 5400 × 5832 km^2 region

213   in Europe, with a 36 × 36 km grid resolution and 14 vertical layers extending up to approximately

214   7.2 km. The modeling period covers 34 days, from June 5 to July 8, 2012 corresponding to the

215   PEGASOS 2012 intensive period. PMCAMx-UF was set to perform simulations on a rotated polar

216   stereographic map projection. The first two days of each simulation were excluded from the

217 analysis to minimize the effect of the initial conditions on the results. For the boundary conditions,

218 constant and relatively low values have been used (Table S2) so that the predicted particle number

219 concentrations over central Europe are determined for all practical purposes by the emissions and

220 corresponding processes simulated by the model. The effect of these boundary conditions on the

221 predicted number concentrations are discussed in Patoulias et al. (2018).

222   Meteorological inputs to PMCAMx-UF include horizontal wind components, vertical

223 diffusivity, temperature, pressure, water vapor, clouds and rainfall. The Weather Research and

224 Forecasting (WRF) model (Skamarock et al., 2005) was used to generate the above inputs. WRF

225 was driven by geographical and dynamic meteorological data generated by the Global Forecast

226 System. Each layer of PMCAMx-UF was aligned with the layers used in WRF. The WRF

227 simulation was periodically re-initialized every 3 days with observed conditions to ensure accuracy

228 in the corresponding fields used as inputs in PMCAMx-UF. The measurements were pre-processed

229 by the WPS (WRF Preprocessing System) package, which provides each atmospheric and static

230 field with fidelity appropriate to the chosen grid resolution of the model. The performance of WRF

231 for Europe against observed meteorological variables has been the topic of several recent studies

232 (Jimenez-Guerrero et al., 2008; de Meij et al., 2009; Im et al., 2010; Argueso et al., 2011; Garcia-

233 Diez et al., 2012) demonstrating good performance.

234   The particle emissions were based on the pan-European anthropogenic particle number

235 emission inventory (Denier van der Gon et al., 2009; Kulmala et al., 2011) and the carbonaceous

236 aerosol inventory (Kulmala et al., 2011) developed during the EUCAARI (European Integrated

237 project on Aerosol, Cloud, Climate, and Air Quality Interactions) project. The resulting

238 number/mass inventories includes both number emissions and consistent size-resolved

239 composition for particles over the size range of approximately 10 nm to 10 μm. Hourly gridded

240 anthropogenic and biogenic emissions included both gases and primary particulate matter. The

241 natural emissions include both particulate matter and gases and combine three different data sets:

242 emissions from ecosystems based on the Model of Emissions of Gases and Aerosols from Nature

243 (MEGAN; Guenther et al., 2006), marine emissions based on the model of O'Dowd et al. (2008)

244 as sea surface covers a considerable area of the domain, and wildfire emissions (Sofiev et al.,

245 2008a, b). MEGAN uses as inputs the plant functional type, the leaf area index, various chemical

246 species emission factors and weather data provided by the WRF. Wind speed fields from WRF

247 and chlorophyll-a concentrations were used as inputs of the marine aerosol model. VOCs were

248 speciated based on the approach proposed by Visschedijk et al. (2007). Anthropogenic gas

249 emissions included land emissions from the GEMS (global and regional Earth-system monitoring

250 using satellite and in-situ data) dataset (Visschedijk et al., 2007). The international shipping,

251 industrial, domestic, agricultural and traffic aerosol emission sources were included in the

252 anthropogenic inventory (Denier van der Gon et al., 2009; Kulmala et al., 2011).

253   The model results were compared against measurements in 26 ground sites, which are

254 available in the European Supersites for Atmospheric Aerosol Research (EUSAAR), and EBAS

255 databases (https://ebas.nilu.no) and the Aerosols, Clouds and Trace gases Research Infrastructure

256 (ACTRIS) (https://actris.nilu.no). Particle size distribution measurements at all sites were made

257 using either a Differential Mobility Particle Sizer (DMPS) or a Scanning Mobility Particle Sizer

258 (SMPS). Information about all stations can be found in Table S3.

259   An intensive field campaign took place in Europe, as part of the Pan-European-Gas-

260 AeroSOl-climate-interaction Study (PEGASOS) project, from June 5 to July 8, 2012.

261 Measurements of aerosol mass concentration PM_1 (particulate matter particles of diameter less

262 than 1 micrometer) from the PEGASOS project are also available for the same period for Patras

263 (Greece), Finokalia (Greece), San Pietro Capofiume (Italy) and Bologna (Italy) (Table S4) and

264 filter $PM_{2.5}$ (particulate matter particles of diameter less than 2.5 micrometer) measurements from

265 6 additional stations in Europe (Table S5). For the calculation of organic mass, we used an average

266 organic mass to organic carbon ratio value equal to 1.8 (Kostenidou et al., 2015).

267   The airborne measurements acquired by the PEGASOS Zeppelin were acquired during the

268 simulation period over the Po Valley. The Po Valley region is situated between the Alps in the

269 north and the Apennines Mountains in the south–southwest. The mountains surround the valley on

270 three sides and high levels of pollutants are often observed in the region due to the industrial,

271 agricultural, and other anthropogenic emissions. In addition, emissions from ship traffic on the

272 Adriatic Sea (Hamed et al., 2007) and long-range transport from central-eastern Europe also

273 contribute pollutants to the region (Sogacheva et al., 2007). A SMPS was used to measure the

274 number size distribution of particles in the size range of 10 to 430 nm. Details of the relevant

275 PEGASOS Zeppelin measurements can be found in Lampilahti et al. (2021).

276

277

278

3. Results

3.1   Base case

The average predicted ground level average number concentrations for the total number of particles (N_{tot}) and for particles with diameters above 10 nm (N_{10}), 50 nm (N_{50}) and 100 nm (N_{100}), during June 5 to July 8, 2012 are shown in Figure 1. The N_{50} and N_{100} concentrations are often used as proxies for CCN number concentrations (Fountoukis et al., 2012). On a domain average basis, the model predicted for the ground level 4780 cm^{-3} for N_{tot}, 3630 cm^{-3} for N_{10}, 1990 cm^{-3} for N_{50}, and 820 cm^{-3} for N_{100} during the simulated period. The highest N_{tot} average concentrations (more than 15000 cm^{-3}) were predicted over Bulgaria, southern Romania, Turkey, Poland, Holland, Portugal, Northern Spain, Eastern UK and Russia. On the other hand, the highest N_{50} and N_{100} are predicted over the Mediterranean, mainly in areas near Southern Spain, Southern Italy, and the Balkans. The N_{tot} and N_{10} are high in areas of frequent nucleation events and areas with high particle number emissions, whereas the N_{50} and N_{100} levels are affected significantly by secondary particulate matter production. The high photochemical activity over the Eastern Mediterranean leads to the corresponding high levels of N_{50} and N_{100} during this period.

3.2 Evaluation of PMCAMx-UF predictions

3.2.1 Comparison of PMCAMx-UF predictions to ground aerosol number observations

The prediction skill metrics of PMCAMx-UF, for the daily average ground measurements from the 26 stations, are summarized in Tables 1 and 2 for both the base case and the case in which the ELVOCs are neglected.

For the base case simulation, the model has a tendency to overestimate the N_{10} levels. The normalized mean bias (NMB) for the daily average concentrations is 23% and the normalized mean error (NME) 63%. The N_{10} was overpredicted in 18 sites, underpredicted in 7 and there was no bias in one. The NMB in 8 sites (Prague-Suchdol, Ispra, Melpitz, Patras, K-Puszta, Hohen-peissenberg, Hyytiala and San Pietro Capofiume) was less than ±15%, and for another 8 stations between ±15% and ±40% (Annaberg-Buchholz, Cabauw, Dresden Nord and Winckelmannstrasse, Finokalia, Giordan Lighthouse, Kosetice, Montseny and Varrio). The highest discrepancies with the measurements of N_{10} were found in Aspvreten, Birkness II, Usti n.L.-mesto, Vavihill, Vielsalm, Zugspitze-Schneefernerhaus, Waldhof, Costa Navarino, and Thesssaloniki with NMB higher than ±40%.

310   The model performed better for N_{100}. There was little bias in the corresponding predictions

311   on average (the NMB was -10%) and the NME was 45%. The NMB for 10 sites (Cabauw, Giordan

312   Lighthouse, Hyytiala, Kosetice, Melpitz, Patras, Prague-Suchdol, Vielsalm, Waldhof and

313   Zugspitze) was less than ±15% and for another 12 (Annaberg-Buchholz, Birkenes II, Dresden

314   Nord and Winckelmannstrasse, Finokalia, Hohenpeissenberg, Ispra, K-Puszta, Montseny, Costa

315   Navarino, San Pietro Capofiume, Usti n.L-mesto. and Vavihill) between ±15% and ±40% (Table

316   2). The absolute NMB for N_{100} exceeded 40% only in Aspvreten, Varrio and Thessaloniki.

3.3.2 Evaluation of aerosol composition predictions

318   The PMCAMx-UF predictions can be evaluated during that period using available PM_1

319   measurements from Aerosol Mass Spectrometers at four stations (Bologna and San Pietro

320   Capofiume, in Italy and Finokalia and Patras, in Greece) that were part of the PEGASOS

321   campaign.

322   In Italy and Greece, the model reproduces the observations of the PM_1 concentrations of

323   the major inorganic aerosol components (sulfate, ammonium, nitrate) reasonably well (Table 3).

324   The model tends to underpredict the organic aerosol concentrations in Patras and Bologna, while

325   it overpredicts the OA in Finokalia and San Pietro Capofiume (Table 4). The OA NMB is -2% and

326   the NME is 38%, with the Finokalia site presenting the higher NMB value (50%) and San Pietro

327   Capofiume, Bologna the lower (±20%) (Table 4).

328   For the rest of Europe, $PM_{2.5}$ filter measurements have been used, available in the European

329   Supersites for Atmospheric Aerosol Research (EUSAAR) and EBAS databases

330   (http://ebas.nilu.no/) for stations that had available data for more than 15 days during the simulated

331   period (6 additional stations in Europe: Payerne, Melpitz, Montseny, Ispra, Diabla Gora, and

332   Iskrba; Table 5). For the calculation of OA mass concentration, we assumed OA:OC=1.8

333   (Kostenidou et al., 2015). For these sites, the model has a tendency towards overestimating the

334    $PM_{2.5}$ OA concentration for 4 out of 6 stations, presenting an average NMB of 20% and NME of

335   62% (Table 5).

3.3.3 Comparison of PMCAMx-UF predictions to Zeppelin measurements

337   One of the challenges of the PMCAMx-UF evaluation using airborne measurements is that

338   the model predictions are available every 15 min while the corresponding measurements by the

339   Zeppelin were taken every 3 min in different heights. For comparison purposes, the model output

340   was interpolated to the times of the Zeppelin measurement periods. PMCAMx-UF reproduced

341   more than 75% of the 2000 3-min N_{10} and N_{100} measurements by the Zeppelin with a factor of 2

342   (Figure S1). The vertical profiles shown in Fig.2, are averages of different flights that collected

343   data in different days and different altitudes each time. The number of samples at different altitudes

344   changed for each flight creating additional variability in the measured profiles.

345   To facilitate the comparison between measurements and predictions the corresponding

346   average profiles (matched in space and time) were calculated using 80 m altitude bins for all the

347   PEGASOS flights. PMCAMx-UF reproduced on average the N_{10} measurements over Po Valley at

348   the lower 160 m and above 400 m, but underestimated the higher N_{10} levels measured in the

349   residual layer at heights between 160-400 m at several of the flights that started several hours

350   before sunrise (Fig. 2a). The average measured N_{10} at all heights was 6,000 cm^{-3}, while the

351   predicted concentration was equal to 4,700 cm^{-3}.

352   PMCAMx-UF reproduced well the N_{100} concentration at all heights (Fig 2b). The model

353   also reproduced 80% of the 3-min N_{100} Zeppelin measurements within a factor of 2. The measured

354   average N_{100} at all heights was 1,500 cm^{-3} and the average predicted by PMCAMx-UF was 1,800

355   cm^{-3}. The ability of the revised model to reproduce reasonably well the high-time resolution (3-

356   minute) Zeppelin measurements at multiple altitudes and locations is encouraging.

357

358   **3.2   Effect of ELVOC production on particle number and OA concentrations**

359   An additional simulation was performed neglecting the production of ELVOCs from

360   terpenes (case 2). The addition of ELVOCs, increased the PM$_{2.5}$ OA mass by approximately as

361   much as 0.5 μg m^{-3} in Central/Eastern Europe and Russia, accounting for approximately 10-15%

362   of the OA (Fig. 3). In these areas a combination of high terpene emissions and high photochemical

363   reaction rates existed during the simulated period. The highest relative predicted increase of OA

364   was 15-25% in northern Europe. In central Europe the ELVOC formation increased average OA

365   by approximately 10%.

366   The average fractional increase of N_x, due to the production of ELVOCs is calculated as:

367     $$f_{Nx} = \frac{N_x(\text{with ELVOCs}) - N_x(\text{without ELVOCs})}{N_x(\text{without ELVOCs})}$$ (1)

368   where, x, is 10, 50, 100 nm or zero (total number). Rather surprisingly, the average fractional

369   change for all number concentrations (N_{tot}, N_{10}, N_{50} and N_{100},) is small ranging between 1% and -

370   4% (Fig. 4) (N_{tot}: -8 cm^{-3} or -0.14%, N_{10}: 40 cm^{-3} or -1.14%, N_{50}: 60 cm^{-3} or 3 %, N_{100}: 35 cm^{-3} or

371   4%). One reason for the small average change is that both increases and decreases are predicted

372   for different areas in Europe. These mixed results are due to the fact that the ELVOC condensation

373   accelerates the growth of new and preexisting particles to larger sizes, but at the same time

374   accelerates their losses due to the increase of the coagulation sink and decreases the nucleation

375   rate due to the increase of the condensation sink.

376   The formation of ELVOCs resulted in a predicted decrease of N_{tot} by 20% (300-600 cm^{-3})

377   in parts of the Nordic countries and by 5% in central Europe (Fig. 4). The decreases are predicted

378   for most Europe with the exception of a few areas in which increases are predicted (northern

379   Iberian Peninsula, parts of France, areas in the Balkans with high sulfur dioxide levels, etc.) (Fig.

380   5). The predicted N_{10} increased by 5-15% (150-400 cm^{-3}) over Finland, northwestern Russia,

381   France, Ireland and northern Portugal. At the same time there were small decreases of a few percent

382   over several areas in Europe especially in the south and in the east as well over the Baltic Sea. N_{50}

383   increased over almost of Europe by 50 to 300 cm^{-3}. This N_{50} increase corresponds to 20-40% over

384   Scandinavia and northwestern Russia, and 10% for central Europe. Finally, the ELVOCs caused

385   an increase in N_{100} of 20-50% over Scandinavia and 10-20% increases over central Europe. The

386   absolute corresponding N_{100} changes in these areas are 100-200 cm^{-3}.

387   The corresponding changes of the number concentrations for particles with diameters

388   between 1 and 10 nm (N_{1-10}), 10 and 50 nm (N_{10-50}) and (iii) 50 and 100 nm (N_{50-100}) are

389   summarized in Fig. S2. These figures illustrate the complex effect of the ELVOCs on different

390   parts of the aerosol number distribution. Decreases in the concentrations of the 1-10 nm particles

391   (decreasing nucleation rate due to increased condensation sink, increasing coagulation with larger

392   particles), increases in the concentrations of the particles larger than 100 nm (due to accelerated

393   growth of the sub-100 nm particles to larger sizes) and both increases and decreases in the 10-50

394   nm size range depending on the magnitude of the different competing processes in each area. The

395   effect of the ELVOCs in this PMCAMx simulation is clearly a lot more complex than a uniform

396   increase of particle number concentrations.

397   The results in the Hyytiala station in Finland were examined in more detail because the

398   predicted number concentrations in Finland are quite sensitive, according to PMCAMx-UF, to the

399   addition of the ELVOCs. The predicted N_3, N_{10}, N_{50} and N_{100} concentrations for the base case are

400   in reasonable agreement with the field measurements in this area (Figure S3), with a tendency of

401   the model to overpredict the N_3 levels during a few nucleation events. For all concentrations the

402   simulation with the ELVOCs (base case) reproduces the measurements better than the simulation

403   in which they are neglected. The condensation sink (CS) for Hyytiala increases by a few percent

404   due to the additional mass of the ELVOCs (Figure S3). The average measured and predicted

405   number size distributions in Hyytiala site (Finland) are shown in Figure S4. The addition of the

406   ELVOCs leads to increased levels in the part of the size distribution above 50 nm. A decrease of

407   the concentration of particles with diameter below 7 nm is predicted due to the addition of the

408   ELVOCs because of both increased coagulation losses but also lower nucleation rates.

409   The ELVOC addition played a minor role on the overall performance of PMCAMx-UF. The

410   NMB for N_{10} decreased (in absolute terms) by 1%, it increased by 5% for N_{100} due to the addition

411   of the ELVOCs in the simulation (Table 1-2). The addition of the ELVOCs affects mainly the

412   PMCAMx-UF predictions in northern Europe and especially Finland, where the predictions of

413   N_{100} significantly improve. In Hyytiala site the NMB decreases from -34% to -14% and in Varrio

414   drops from -72% to -49%. The corresponding normalized mean errors changed by 1-2%. These

415   small changes in the performance metrics are consistent with the small overall changes caused by

416   the ELVOC addition.

417   The small change in the OA mass concentration due to the addition of the ELVOCs has a

418   modest impact on the performance of PMCAMx-UF for OA (Table S6 and S7). For example, the

419   PM_1 OA bias improves from -6% to 2% while the $PM_{2.5}$ OA bias increases from 15% to 20%. The

420   changes in normalized error are 1% or less.

421

3.3   Effect of IVOCs on particle number concentrations

423   The emissions of IVOCs ($C^* \geq 10^{-3}$ μg m^{-3}) were set to zero in a sensitivity test (Case 3) to

424   quantify their effect on the predicted particle number concentration and size distribution. The

425   SOA formed by the IVOCs (SOA-iv) exceeds 1 μg m^3 in southern Europe, over the Mediterranean

426   Sea, but also in large areas over central and eastern Europe (Fig. 6). The high SOA-iv levels over

427   the Mediterranean are due to the oxidation of IVOCs emitted from large wildfires that occurred

428   during the simulation period. The corresponding SOA-iv is 10-25% of the total OA over

429   continental Europe and even higher (about 60%) over parts of the marine atmosphere.

430   According to PMCAMx-UF the addition of the emissions of IVOCs and their aging

431   reactions lead to a reduction of N_{tot} by 5-10% and N_{10} by 5% (Fig. 7) for continental Europe. On

432   the other hand, this addition of IVOCs leads to an increase of N_{50} by 5% and N_{100} by 5-10% mainly

433 in central Europe and the Mediterranean Sea (Fig. 7). The corresponding changes of the number

434 concentrations for the various size ranges $N_{1–10}$, $N_{10–50}$ and $N_{50–100}$ are summarized in Fig. 8. The

435 predicted $N_{1–10}$ decreases approximately 15-20% for most of Europe except for the Scandinavian

436 peninsula due to the IVOCs. $N_{10–50}$ decreases 10-15% mainly in southern Europe and $N_{50–100}$

437 changes less than ±5% or ±100 cm^{-3} in the simulated domain.

438  The atmospheric oxidation of the emitted IVOCs produces semi-volatile organic

439 compounds, which condense preferentially on particles in the accumulation mode and not so much

440 on the smallest particles due to the Kelvin effect. This results in an increase of both the

441 condensation and coagulation sinks, which then lead to a decrease of the nucleation rate but also

442 on the coagulation rate of the smaller with the larger particles.

443  The effect of the addition of the IVOCs on the performance of PMCAMx-UF is modest and

444 mixed. The NMB for N_{10} increased by 4% (from 23% to 27%) and decreased by 5% for N_{100} (from

445 10% to 5%) (Table S5). The corresponding NME for both N_{10} and N_{100} changed slightly

446 (approximately 1%). The modest overall changes on the number distribution of the ultrafine

447 particles caused by the addition of IVOCs and the corresponding aging reactions are consistent

448 with the small changes in the PMCAMx-UF performance metrics.

449  The addition of the IVOCs and the resulting SOA-iv from their oxidation also had mixed

450 results in the PMCAMx-UF performance for OA in Europe. This added SOA removed the

451 underprediction of OA against the AMS measurements in Italy and Greece; the NMB changed

452 from -18% when IVOCs were neglected to 2% when IVOCs were included (Table S8). The NME

453 increased a little (from 35% to 35%) with the IVOC addition. The performance against the OA

454 measurements in the other European sites became a little worse when IVOCs were included in the

455 model (Table S9). The small underprediction (NMB=-8%) in OA became a larger overprediction

456 (NMB=20%) and the NME increased from 50% to 62%. These results are characteristic of the

457 uncertainties in primary OA emissions but also SOA production from the various VOCs and

458 IVOCs emitted by anthropogenic and biogenic sources.

459

460 **4. Conclusions**

461  A new version of PMCAMx-UF was developed with the ability to simulate the formation

462 and dynamic condensation of ELVOCs during the oxidation of the monoterpenes and the

463 emissions and multi-generational chemistry of IVOCs. The model was applied to the PEGASOS

464   summer intensive period campaign during the summer of 2012. The available measurements

465   included both ground stations across Europe and airborne measurements from a Zeppelin over the

466   Po Valley.

467   The number concentration predictions of PMCAMx-UF, are compared against ground

468   measurements from 26 stations in Europe. The model tends to overestimate daily average N_{10} with

469   a normalized bias of 35% and an average error of 64%. PMCAMx-UF performed well for N_{100}

470   with a low bias (-2 %) and an error of 41%. The performance of the model in the lowest 1 km of

471   the atmosphere above Po Valley for both N_{10} and N_{100} was even better than its average performance

472   over Europe. The model's predicted PM_1 and $PM_{2.5}$ concentrations and composition had NMB of

473   15% and errors less than 60% depending on the PM component. These results suggest that

474   PMCAMx-UF does a reasonable job reproducing the aerosol mass and number concentrations over

475   Europe during the simulated period.

476   The ELVOCs produced by the monoterpene oxidation contributed, according to the

477   PMCAMx-UF predictions on average around 0.5 μg m^{-3} and accounted for 10-15% of the $PM_{2.5}$

478   OA. The highest relative predicted increase of OA was 15-25% in northern Europe, while the

479   ELVOC formation increased average OA by approximately 10% in central Europe.

480   The ELVOC production by monoterpenes led to surprisingly small changes of the average

481   number concentrations over Europe. The total number concentration decreased by 0.2%, the N_{10}

482   decreases by 1.1%, while N_{50} increased by 3% and N_{100} by 4% due to this new SOA source. One

483   of the reasons for these small average increases is the nonlinearity of the system leading to both

484   increases and decreases in different parts of Europe. Even if ELVOCs accelerate the growth of the

485   newly formed particles to larger sizes increasing in this way their lifetime, at the same time they

486   increase the aerosol mass and surface area as they mostly condense on the accumulation mode.

487   Therefore, they increase the condensation sink, decreasing the sulfuric acid supersaturation and

488   the corresponding nucleation rate. They also increase the coagulation sink and thus accelerate the

489   removal of all nanoparticles.

490   Locally the effects of the ELVOC production could be higher. For example, it is estimated

491   that the ELVOC productions leads to a decrease of the total particle concentration N_{tot} by 20% in

492   parts of the Nordic countries and by 5% in central Europe. At the same time, the predicted N_{10}

493   increased by 5-15% (150-400 cm^{-3}) over Finland, northwestern Russia, France, Ireland and

494   northern Portugal due to these secondary organic compounds. The predicted N_{50} increased almost

495 everywhere in continental Europe by 50-300 cm^{-3}. This is 10% increase of N_{50} over central Europe

496 and 20-40% over Scandinavia and northwestern Russia.

497   The addition of IVOC emissions and their aging reactions led to surprising reduction of the

498 total number of particles (N_{tot}) and N_{10} by 10-15 and 5-10%, respectively, and to an increase of the

499 concentration of N_{100} by 5-10%. In this case semi-volatile organic mass is produced, which

500 condenses preferentially on particles in the accumulation mode, increasing the condensation and

501 coagulation sinks and leading to a decrease in the concentration of the sub-10 nm particles.

502

503 **Data and code availability.** Field measurement data are available in ebas.nilu.no and

504 https://actris.nilu.no/. The Zeppelin-relevant, San Pietro Capofume and Bologna data are available

505 in https://doi.org/10.5281/zenodo.4660145 (Lampilahti et al. 2021). The field datasets for Patras,

506 Thessaloniki and Costa Navarino can be obtained after request to the authors. The PMCAMx-UF

507 is available from the authors (spyros@chemeng.upatras.gr).

508
509 **Supplement.**

510

511 **Author contributions.** DP wrote the code, conducted the simulations, analyzed the results, and

512 wrote the paper. SNP was responsible for the design of the study and the synthesis of the results

513 and contributed to the writing of the paper.

514

515 **Competing interests.** The authors declare that they have no conflict of interest.

516

517 **Acknowledgments**: The authors would like to thank the PEGASOS team and the members and

518 personnel of ACTRIS measurement sites. The ACTRIS project has received funding from

519 the European Union Seventh Framework Programme (ACTRIS, FP7/2007-2013, grant agreement

520 no. 262254) and the ACTRIS-2 project has received funding from the European Union's Horizon

521 2020 research and innovation programme under grant agreement No 654109. We would like to

522 especially thank: Pasi Aalto, Andres Alastuey, Benjamin Bergmans, Wolfram Birmili, Miroslav

523 Bitter, Raymond Ellul, Markus Fiebig, Harald Flentje, Spiridon Bezantakos, George Biskos,

524 Evangelos Gerasopoulos, Johannes Groess, Bas Henzing, Nikos Kalivitis, Hans Karlsson,

525 Evangelia Kostenidou, Giorgos Kouvarakis, Markku Kulmala, Fabian Lenartz, Gunter Loeschau,

526 Chris Lunder, Nikos Mihalopoulos, Marcel Moerman, David Munao, Colin O'Dowd, Noemi

Perez, Helena Placha, Jean-Philippe Putaud, Alexander Schladitz, Franz Rohrer, Erik Swietlicki,

Ralf Tillmann, Thomas Tuch, Kay Weinhold, Alfred Wiedensohler, Vladimir Zdimal, Hans-

Christen Hansson, Peter Tunved and Radovan Krejci for the results of the field measurementa.

Financial support: This work was supported by the project FORCeS funded from the European

Union's Horizon 2020 research and innovation programme under grant agreement No 821205. We

also acknowledge support by the project by the Greek PERAN project MIS 5002358.

References

Adams, P. J. and Seinfeld, J. H.: Predicting global aerosol size distributions in general circulation
models, J. Geophys. Res., 107, 4370, https://doi.org/10.1029/2001JD001010, 2002.

Argueso, D., Hidalgo-Munoz, J. M., Gamiz-Fortis, S. R., and Esteban-Parra, M. J.: Evaluation of
WRF parameterizations for climate studies over Southern Spain using a multistep regional-
ization, J. Climate, 24, 5633–5651, 2011.

Atkinson, R.: Atmospheric chemistry of VOCs and NO_x, Atmos. Environ., 34, 2063–2101, 2000.

Atkinson, R. and Arey, J.: Atmospheric degradation of volatile organic compounds, Chem. Rev.,
103, 4605–4638, doi:10.1021/cr0206420, 2003.

Carter, W. P. L.: Programs and files implementing the SAPRC-99 mechanism and its associates
emissions processing procedures for Models-3 and other regional models, January 31, 2000.

Dahneke, B.: Simple Kinetic Theory of Brownian Diffusion in Va- pors and Aerosols, Theory of
Dispersed Multiphase Flow, edited by Meyer, R. E., Academic Press, New York, 97–133 pp.,
1983.

Dal Maso, M., Kulmala, M., Riipinen, I., Wagner, R., Hussein, T., Aalto, P., and Lehtinen, K. E.
J.: Formation and growth of fresh atmospheric aerosols: eight years of aerosol size distribution
data from SMEAR II, Hyytiälä, Finland, Boreal Environ. Res., 10, 323–336, 2005.

de Gouw, J. A., et al.: Budget of organic carbon in a polluted atmosphere: Results from the New
England Air Quality Study in 2002, J. Geophys. Res., 110, D16305, doi:10.1029/
2004JD005623, 2005.

de Meij, A., Gzella, A., Cuvelier, C., Thunis, P., Bessagnet, B., Vinuesa, J. F., Menut, L., and
Kelder, H. M.: The im- pact of MM5 and WRF meteorology over complex terrain on
CHIMERE model calculations, Atmos. Chem. Phys., 9, 6611– 6632, 2009.

558 Denier van der Gon, H. A. C., Visschedijk, A. J. H., Johansson, C., Hedberg Larsson, E., Harrison,
559   R., and Beddows, D.: Size resolved pan European anthropogenic particle number inventory,
560   EUCAARI Deliverable report D141 (available on request from EUCAARI project office),
561   TNO, the Netherlands, 2009.

562 Docherty, K. S. et al.: Apportionment of Primary and Secondary Organic Aerosols in Southern
563   California during the 2005 Study of Organic Aerosols in Riverside (SOAR-1), Environ. Sci.
564   Technol., 42, 7655–7662, 2008.

565 Donahue, N. M., Robinson, A. L., Stanier, C. O., Pandis, S. N.: Coupled partitioning, dilution, and
566   chemical aging of semivolatile organics, Environ. Sci. Technol., 40, 2635-2643, 2006.

567 Donahue, N. M., Epstein, S. A., Pandis, S. N., and Robinson, A. L.: A two-dimensional volatility
568   basis set: 1. organic-aerosol mixing thermodynamics, Atmos. Chem. Phys., 11, 3303–3318,
569   doi:10.5194/acp-11-3303-2011, 2011.

570 Dzepina, K., Volkamer, R. M., Madronich, S., Tulet, P., Ulbrich, I. M., Zhang, Q., Cappa, C. D.,
571   Ziemann, P. J., and Jimenez, J. L.: Evaluation of recently-proposed secondary organic aerosol
572   models for a case study in Mexico City, Atmos. Chem. Phys., 9, 5681-5709, 2009.

573 Ehn, M., Thornton, J. A., Kleist, E., Sipilä, M., Junninen, H., Pulli- nen, I., Springer, M., Rubach,
574   F., Tillmann, R., Lee, B., Lopez- Hilfiker, F., Andres, S., Acir, I. H., Rissanen, M., Jokinen,
575   T., Schobesberger, S., Kangasluoma, J., Kontkanen, J., Nieminen, T., Kurtén, T., Nielsen, L.
576   B., Jørgensen, S., Kjaergaard, H. G., Canagaratna, M., Dal Maso, M., Berndt, T., Petäjä, T.,
577   Wahner, A., Kerminen, V. M., Kulmala, M.,Worsnop, D. R., Wildt, J., and Mentel, T. F.: A
578   large source of low-volatility secondary organic aerosol, Nature, 506, 476–479, 2014.

579 Environ, User's guide to the comprehensive air quality model with extensions (CAMx), version
580   4.02, report, ENVIRON Int. Corp., Novato, Calif, 2003.

581 Fanourgakis, G. S., Kanakidou, M., Nenes, A., Bauer, S. E., Bergman, T., Carslaw, K. S., Grini,
582   A., Hamilton, D. S., Johnson, J. S., Karydis, V. A., Kirkevåg, A., Kodros, J. K., Lohmann, U.,
583   Luo, G., Makkonen, R., Matsui, H., Neubauer, D., Pierce, J. R., Schmale, J., Stier, P.,
584   Tsigaridis, K., van Noije, T., Wang, H., Watson-Parris, D., Westervelt, D. M., Yang, Y.,
585   Yoshioka, M., Daskalakis, N., Decesari, S., Gysel-Beer, M., Kalivitis, N., Liu, X., Mahowald,
586   N. M., Myriokefalitakis, S., Schrödner, R., Sfakianaki, M., Tsimpidi, A. P., Wu, M., and Yu,
587   F.: Evaluation of global simulations of aerosol particle and cloud condensation nuclei number,
588   with implications for cloud droplet formation, Atmos. Chem. Phys., 19, 8591–8617, 2019.

589 Fountoukis, C., Riipinen, I., Denier Van Der Gon, H. A. C., Charalampidis, P. E., Pilinis, C.,
590   Wiedensohler, A., O'Dowd, C., Putaud, J. P., Moerman, M. and Pandis, S. N.: Simulating
591   ultrafine particle formation in Europe using a regional CTM: Contribution of primary
592   emissions versus secondary formation to aerosol number concentrations, Atmos. Chem. Phys.,
593   12, 8663–8677, 2012.

594 Garcia-Diez, M., Fernandez, J., Fita, L., and Yague, C.: Sea- sonal dependence of WRF model
595   biases and sensitivity to PBL schemes over Europe, Q. J. Roy. Meteor. Soc., 139, 501–514,
596   2012.

597 Gaydos, T. M., Stainer, C. O., and Pandis, S. N.: Modeling of in-situ ultrafine atmospheric particle
598   formation in the eastern United State, J. Geophys. Res., 110, D07S12, https://doi.org/10.1029/
599   2004JD004683, 2005.

600 Gaydos, T., Pinder, R., Koo, B., Fahey, K., Yarwood, G., and Pan- dis, S. N.: Development and
601   application of a three-dimensional Chemical Transport Model, PMCAMx, Atmos. Environ.,
602   41, 2594–2611, 2007.

603 Gordon, H., Sengupta, K., Rap, A., Duplissy, J., Frege, C., Williamson, C., Heinritzi, M., Simon,
604   M., Yan, C., Almeida, J., Tröstl, J., Nieminen, T., Ortega, I. K., Wagner, R., Dunne, E. M.,
605   Adamov, A., Amorim, A., Bernhammer, A.-K., Bianchi, F., Breitenlechner, M., Brilke, S.,
606   Chen, X., Craven, J. S., Dias, A., Ehrhart, S., Fischer, L., Flagan, R. C., Franchin, A., Fuchs,
607   C., Guida, R., Hakala, J., Hoyle, C. R., Jokinen, T., Junninen, H., Kangasluoma, J., Kim, J.,
608   Kirkby, J., Krapf, M., Kürten, A., Laaksonen, A., Lehtipalo, K., Makhmutov, V., Mathot, S.,
609   Molteni, U., Monks, S. A., Onnela, A., Peräkylä, O., Piel, F., Petäjä, T., Praplan, A. P., Pringle,
610   K. J., Richards, N. A. D., Rissanen, M. P., Rondo, L., Sarnela, N., Schobesberger, S., Scott, C.
611   E., Seinfeld, J. H., Sharma, S., Sipilä, M., Steiner, G., Stozhkov, Y., Stratmann, F., Tomé, A.,
612   Virtanen, A., Vogel, A. L., Wagner, A. C., Wagner, P. E., Weingartner, E., Wimmer, D.,
613   Winkler, P. M., Ye, P., Zhang, X., Hansel, A., Dom- men, J., Donahue, N. M., Worsnop, D.
614   R., Baltensperger, U., Kulmala, M., Curtius, J., and Carslaw, K. S.: Reduced anthropogenic
615   aerosol radiative forcing caused by biogenic new particle formation, P. Natl. Acad. Sci. USA,
616   113, 12053–12058, 2016.

617 Guenther, A., Karl, T., Harley, P., Wiedinmyer, C., Palmer, P. I., and Geron, C.: Estimates of
618   global terrestrial isoprene emissions using MEGAN (Model of Emissions of Gases and
619   Aerosols from Nature), Atmos. Chem. Phys., 6, 3181–3210, 2006.

620 Hallquist, M., Wenger, J. C., Baltensperger, U., Rudich, Y., Simpson, D., Claeys, M., Dommen,
621   J., Donahue, N. M., George, C., Goldstein, a. H., Hamilton, J. F., Herrmann, H., Hoffmann,
622   T., Iinuma, Y., Jang, M., Jenkin, M. E., Jimenez, J. L., Kiendler-Scharr, a., Maenhaut, W.,
623   McFiggans, G., Mentel, T. F., Monod, A., Prévôt, A. S. H., Seinfeld, J. H., Surratt, J. D.,
624   Szmigielski, R. and Wildt, J.: The formation, properties and impact of secondary organic
625   aerosol: current and emerging issues, Atmos. Chem. Phys., 9, 5155–5236, 2009.

626 Hamed, A., Joutsensaari, J., Mikkonen, S., Sogacheva, L., Dal Maso, M., Kulmala, M., Cavalli,
627   F., Fuzzi, S., Facchini, M. C., Decesari, S., Mircea, M., Lehtinen, K. E. J., and Laaksonen, A.:
628   Nucleation and growth of new particles in Po Valley, Italy, Atmos. Chem. Phys., 7, 355–376,
629   2007.

630 Im, U., Markakis, K., Unal, A., Kindap, T., Poupkou, A., Incecik, S., Yenigun, O., Melas, D.,
631   Theodosi, C., and Mihalopoulos, N.: Study of a winter PM episode in Istanbul using the high
632   resolution WRF/CMAQ modeling system, Atmos. Environ., 44, 3085–3094, 2010.

633 Jimenez-Guerrero, P., Jorba, O., Baldasano, J. M., and Gasso, S.: The use of a modelling system
634   as a tool for air quality management: Annual high-resolution simulations and evaluation, Sci.
635   Total Environ., 390, 323–340, 2008.

636 Jokinen, T., Berndt, T., Makkonen, R., Kerminen, V.-M., Jun- ninen, H., Paasonen, P., Stratmann,
637   F., Herrmann, H., Guenther, A. B., Worsnop, D. R., Kulmala, M., Ehn, M., and Sipilä, M.:
638   Production of extremely low volatile organic com- pounds from biogenic emissions: Measured
639   yields and atmospheric implications, P. Natl. Acad. Sci. USA, 112, 7123–7128, 2015.

640 Jung, J., Adams, P. J., and Pandis, S. N.: Simulating the size distribution and chemical composition
641   of ultrafine particles during nucleation events, Atmos. Environ., 40, 2248–2259, 2006.

642 Jung, J. G., Fountoukis, C., Adams, P. J. and Pandis, S. N.: Simulation of in situ ultrafine particle
643   formation in the eastern United States using PMCAMx-UF, J. Geophys. Res., 115, D03203,
644   doi: 10.1029/2009jd012313, 2010.

645 Kanakidou, M., Seinfeld, J. H., Pandis, S. N., Barnes, I., Dentener, F. J., Facchini, M. C., Van
646   Dingenen, R., Ervens, B., Nenes, A., Nielsen, C. J., Swietlicki, E., Putaud, J. P., Balkanski, Y.,
647   Fuzzi, S., Horth, J., Moortgat, G. K., Winterhalter, R., Myhre, C. E. L., Tsigaridis, K., Vignati,
648   E., Stephanou, E. G., and Wilson, J.: Organic aerosol and global climate modelling: a review,
649   Atmos. Chem. Phys., 5, 1053–1123, 2005.

650 Karydis, V. A., Tsimpidi, A. P., and Pandis, S. N.: Evaluation of a three-dimensional chemical
651   transport model (PMCAMx) in the eastern United States for all four seasons, J. Geophys. Res.,
652   112, D14211, https://doi.org/10.1029/2006JD007890, 2007.

653 Kirkby, J., Duplissy, J., Sengupta, K., Frege, C., Gordon, H., Williamson, C., Heinritzi, M., Simon,
654   M., Yan, C., Almeida, J., Tröstl, J., Nieminen, T., Ortega, I. K., Wagner, R., Adamov, A.,
655   Amorim, A., Bernhammer, A.-K., Bianchi, F., Breitenlechner, M., Brilke, S., Chen, X.,
656   Craven, J., Dias, A., Ehrhart, S., Flagan, R. C., Franchin, A., Fuchs, C., Guida, R., Hakala, J.,
657   Hoyle, C. R., Jokinen, T., Junninen, H., Kangasluoma, J., Kim, J., Krapf, M., Kürten, A.,
658   Laaksonen, A., Lehtipalo, K., Makhmutov, V., Mathot, S., Molteni, U., Onnela, A., Peräkylä,
659   O., Piel, F., Petäjä, T., Praplan, A. P., Pringle, K., Rap, A., Richards, N. A. D., Riip- inen, I.,
660   Rissanen, M. P., Rondo, L., Sarnela, N., Schobesberger, S., Scott, C. E., Seinfeld, J. H., Sipilä,
661   M., Steiner, G., Stozhkov, Y., Stratmann, F., Tomé, A., Virtanen, A., Vogel, A. L., Wag- ner,
662   A. C., Wagner, P. E., Weingartner, E., Wimmer, D., Winkler, P. M., Ye, P., Zhang, X., Hansel,
663   A., Dommen, J., Donahue, N. M., Worsnop, D. R., Baltensperger, U., Kulmala, M., Carslaw,
664   K. S., and Curtius, J.: Ion-induced nucleation of pure biogenic particles, Nature, 533, 521–526,
665   https://doi.org/10.1038/nature17953, 2016.

666 Kleinman, L. I., Springston, S. R., Daum, P. H., Lee, Y.-N., Nunnermacker, L. J., Senum, G. I.,
667   Wang, J., Weinstein-Lloyd, J., Alexander, M. L., Hubbe, J., Ortega, J., Canagaratna, M. R.,
668   and Jayne, J.: The time evolution of aerosol composition over the Mexico City plateau, Atmos.
669   Chem. Phys., 8, 1559–1575, doi:10.5194/acp-8-1559-2008, 2008.

670 Kostenidou, E., Florou, K., Kaltsonoudis, C., Tsiflikiotou, M., Vratolis, S., Eleftheriadis, K., and
671   Pandis, S. N.: Sources and chemical characterization of organic aerosol during the summer in
672   the eastern Mediterranean, Atmos. Chem. Phys., 15, 11355–11371, 2015.

673 Kroll, J. H., Ng, N. L., Murphy, S. M., Flagan, R. C., Seinfeld, J. H.: Secondary organic aerosol
674   formation from isoprene photooxidation, Environ. Sci. Technol., 40, 155-162, 2006.

675 Kulmala, M., Vehkamaki, H., Petaja, T., Dal Maso, M., Lauri, A., Kerminen, V.-M., Birmili, W.,
676   and McMurry, P. H.: Formation and growth of ultrafine atmospheric particles: A review of
677   observations, J. Aerosol Sci., 35, 143–176, 2004.

678 Kulmala, M., Asmi, A., Lappalainen, H. K., Baltensperger, U., Brenguier, J.-L., Facchini, M. C.,
679   Hansson, H.-C., Hov, Ø., O'Dowd, C. D., Pöschl, U., Wiedensohler, A., Boers, R.,Ammann,
680   M., Arabas, S., Artaxo, P., Baars, H., Beddows, D. C. S., Bergström, R., Beukes, J. P., Bilde,

681 M., Burkhart, J. F., Canonaco, F., Clegg, S. L., Coe, H., Crumeyrolle, S., D'Anna, B., Decesari,

682 S., Gilardoni, S., Fischer, M., Fjaeraa, A. M., Fountoukis, C., George, C., Gomes, L., Halloran,

683 P., Hamburger, T., Harrison, R. M., Herrmann, H., Hoffmann, T., Hoose, C., Hu, M.,

684 Hyvärinen, A., Hõrrak, U., Iinuma, Y., Iversen, T., Josipovic, M., Kanakidou, M., Kiendler-

685 Scharr, A., Kirkevåg, A., Kiss, G., Klimont, Z., Kolmonen, P., Komppula, M., Kristjánsson,

686 J.-E., Laakso, L., Laaksonen, A., Labonnote, L., Lanz, V. A., Lehtinen, K. E. J., Rizzo, L. V.,

687 Makkonen, R., Manninen, H. E., McMeeking, G., Merikanto, J., Minikin, A., Mirme, S.,

688 Morgan, W. T., Nemitz, E., O'Donnell, D., Panwar, T. S., Pawlowska, H., Petzold, A., Pienaar,

689 J. J., Pio, C., Plass-Duelmer, C., Prévôt, A. S. H., Pryor, S., Reddington, C. L., Roberts, G.,

690 Rosen- feld, D., Schwarz, J., Seland, Ø., Sellegri, K., Shen, X. J., Shiraiwa, M., Siebert, H.,

691 Sierau, B., Simpson, D., Sun, J. Y., Topping, D., Tunved, P., Vaattovaara, P., Vakkari, V.,

692 Veefkind, J. P., Visschedijk, A., Vuollekoski, H., Vuolo, R., Wehner, B., Wildt, J., Woodward,

693 S., Worsnop, D. R., van Zadelhoff, G.- J., Zardini, A. A., Zhang, K., van Zyl, P. G., Kerminen,

694 V.- M., S Carslaw, K., and Pandis, S. N.: General overview: Euro- pean Integrated project on

695 Aerosol Cloud Climate and Air Quality interactions (EUCAARI) – integrating aerosol research

696 from nano to global scales, Atmos. Chem. Phys., 11, 13061–13143,

697 https://doi.org/10.5194/acp-11-13061-2011, 2011.

698 Lampilahti, J., Manninen, H. E., Nieminen, T., Mirme, S., Ehn, M., Pullinen, I., Leino, K.,

699 Schobesberger, S., Kangasluoma, J., Kontkanen, J., Järvinen, E., Väänänen, R., Yli-Juuti, T.,

700 Krejci, R., Lehtipalo, K., Levula, J., Mirme, A., Decesari, S., Tillmann, R., Worsnop, D. R.,

701 Rohrer, F., Kiendler-Scharr, A., Petäjä, T., Kerminen, V.-M., Mentel, T. F., and Kulmala, M.:

702 Zeppelin-led study on the onset of new particle formation in the planetary boundary layer,

703 Atmos. Chem. Phys. Discuss. [preprint], https://doi.org/10.5194/acp-2021-282, in review,

704 2021.

705 Lane, T. E., Donahue, N. M., and Pandis, S. N.: Simulating secondary organic aerosol formation

706 using the volatility basis-set approach in a chemical transport model, Atmos. Environ., 42,

707 7439–7451, 2008.

708 Makkonen, R., Asmi, A., Korhonen, H., Kokkola, H., Järvenoja, S., Räisänen, P., Lehtinen, K. E.

709 J., Laaksonen, A., Kerminen, V.- M., Järvinen, H., Lohmann, U., Bennartz, R., Feichter, J.,

710 and Kulmala, M.: Sensitivity of aerosol concentrations and cloud properties to nucleation and

711   secondary organic distribution in ECHAM5-HAM global circulation model, Atmos. Chem.

712   Phys., 9, 1747–1766, https://doi.org/10.5194/acp-9-1747-2009, 2009.

713 Mann, G. W., Carslaw, K. S., Spracklen, D. V., Ridley, D. A., Manketelow, P. T., Chipperfield,

714   M. P., Pickering, S. J., and Johnson, C. E.: Description and evaluation of GLOMAP-mode: A

715   modal global aerosol microphysics model for the UKCA composition-climate model. Geosci.

716   Model Dev., 3, 519-551, 2010.

717 Matsui, H., et al.: Secondary organic aerosol formation in urban air: Temporal variations and

718   possible contributions from unidentified hydrocarbons, J. Geophys. Res., 114, D04201,

719   doi:10.1029/2008JD010164, 2009.

720 Merikanto, J., Spracklen, D. V., Mann, G. W., Pickering, S. J., and Carslaw, K. S.: Impact of

721   nucleation on global CCN, Atmos. Chem. Phys., 9, 8601–8616, https://doi.org/10.5194/acp-9-

722   8601- 2009, 2009.

723 Murphy, B. N., Pandis, S. N. and Ave, F.: Simulating the formation of semivolatile primary and

724   secondary organic aerosol in a regional chemical transport model gas-phase chemistry of OA

725   species, Environ. Sci. Technol., 43, 4722–4728, 2009.

726 Napari, I., Noppel, M., Vehkamaki, H., and Kulmala, M.: Parameterization of ternary nucleation

727   rates for H2SO4-NH3- H2O vapors, J. Geophys. Res., 107, AAC 6-1–AAC 6-6,

728   https://doi.org/10.1029/2002JD002132, 2002.

729 Ng, N. L., Kroll, J. H., Keywood, M. D., Bahreini, R., Varutbangkul, V., Flagan, R. C., Seinfeld,

730   J. H.: Contribution of first- versus second-generation products to secondary organic aerosols

731   formed in the oxidation of biogenic hydrocarbons, Environ. Sci. Technol., 40, 2283-2297, 2006

732 Odum, J. R., Hoffmann, T., Bowman, F. A., Collins, D., Flagan, R. C., Seinfeld, J. H.: Gas/particle

733   partitioning and secondary organic aerosol yields, Environ. Sci. Technol., 30, 2580-2585,

734   1996.

735 O'Dowd, C. D., Langmann, B., Varghese, S., Scannell, C., Ceburnis, D., and Facchini, M. C.: A

736   combined organic-inorganic sea-spray source function, Geophys. Res. Lett., 35, L01801,

737   https://doi.org/10.1029/2007GL030331, 2008.

738 Olenius, T., Yli-Juuti, T., Elm, J, Kontkanen, J., and Riipinen I. New particle formation and

739   growth: creating a new atmospheric phase interface. In Physical Chemistry of Gas-Liquid

740   Interfaces (eds. Faust, J. A. & House, J. E.), 315–352, Elsevier, 2018.

741 Pathak, R. K., Presto, A. A., Lane, T. E., Stanier, C. O., Donahue, N. M., Pandis, S. N.: Ozonolysis
742   of α-pinene: parameterization of secondary organic aerosol mass fraction, Atmos. Chem.
743   Phys., 7, 3811–3821, 2007.

744 Patoulias, D., Fountoukis, C., Riipinen, I., and Pandis, S. N.: The role of organic condensation on
745   ultrafine particle growth during nucleation events, Atmos. Chem. Phys., 15, 6337–6350,
746   https://doi.org/10.5194/acp-15-6337-2015, 2015.

747 Patoulias, D., Fountoukis, C., Riipinen, I., Asmi, A., Kulmala, M., and Pandis, S. N.: Simulation
748   of the size-composition distribution of atmospheric nanoparticles over Europe, Atmos. Chem.
749   Phys., 18, 13639–13654, https://doi.org/10.5194/acp-18-13639-2018, 2018.

750 Pierce, J. R. and Adams, P. J.: A computationally efficient aerosol nucleation/condensation
751   method: Pseudo-steady state sulfuric acid, Aerosol Sci. Tech., 43, 216–226, 2009

752 Pierce, J. R., Riipinen, I., Kulmala, M., Ehn, M., Petäjä, T., Junninen, H., Worsnop, D. R., and
753   Donahue, N. M.: Quantification of the volatility of secondary organic compounds in ultrafine
754   particles during nucleation events, Atmos. Chem. Phys., 11, 9019–9036,
755   https://doi.org/10.5194/acp-11-9019-2011, 2011.

756 Presto, A. A., Donahue, N. M.: Investigation of a-pinene+ozone secondary organic aerosol
757   formation at low total aerosol mass. Environ. Sci. Technol., 40, 3536–3543, 2006.

758 Rissanen, M. P., Kurtén, T., Sipilä, M., Thornton, J. A., Kangasluoma, J., Sarnela, N., Junninen,
759   H., Jørgensen, S., Schallhart, S., Kajos, M. K., Taipale, R., Springer, M., Mentel, T. F., Ruuska-
760   nen, T., Petäjä, T., Worsnop, D. R., Kjaergaard, H. G., and Ehn, M.: The formation of highly
761   oxidized multifunctional products in the ozonolysis of cyclohexene, J. Am. Chem. Soc., 136,
762   15596–15606, 2014.

763 Robinson, A. L., Donahue, N. M., Shrivastava, M. K., Weitkamp, E. A., Sage, A. M., Grieshop,
764   A. P., Lane, T. E., Pandis, S. N., Pierce, J. R.: Rethinking organic aerosols: semivolatile
765   emissions and photochemical aging, Science, 315, 1259-1262, 2007.

766 Schulze, B. C., Wallace, H. W., Flynn, J. H., Lefer, B. L., Erickson, M. H., Jobson, B. T., Dusanter,
767   S., Griffith, S. M., Hansen, R. F., Stevens, P. S., VanReken, T., and Griffin, R. J.: Differences
768   in BVOC oxidation and SOA formation above and below the forest canopy, Atmos. Chem.
769   Phys., 17, 1805–1828, https://doi.org/10.5194/acp-17-1805-2017, 2017.

770 Seinfeld, J. H.; Pandis S. N. Atmospheric Chemistry and Physics: From Air Pollution to Climate
771   Change, 2nd ed.; John Wiley and Sons, Hoboken, NJ, 2006.

772   Sengupta, K., Pringle, K., Johnson, J. S., Reddington, C., Browse, J., Scott, C. E., and Carslaw,
773   K.: A global model perturbed parameter ensemble study of secondary organic aerosol
774   formation, Atmos. Chem. Phys., 21, 2693–2723, https://doi.org/10.5194/acp-21-2693-2021,
775   2021.
776   Shrivastava, M. K., Lane, T. E., Donahue, N. M., Pandis, S. N., and Robinson, A. L.: Effects of
777   gas-particle partitioning and aging of primary emissions on urban and regional organic aerosol
778   concentrations, J. Geophys. Res., 113, D18301, doi:10.1029/2007JD009735, 2008.
779   Shrivastava, M., Thornton, J., Cappa, C., Fan, J., Goldstein, A., Guenther, A., Jimenez, J. L.,
780   Kuang, C., Laskin, A., Martin, S., Ng, N. L., Petaja, T., Pierce, J., Rasch, P., Roldin, P.,
781   Seinfeld, J., Shilling, J., Smith, J., Volkamer, R., Wang, J., Worsnop, D., Zaveri, R., Zelenyuk,
782   A., and Zhang, Q.: Recent advances in understanding secondary organic aerosols: implications
783   for global climate forcing, Rev. Geophys., 55, 509-559, 2017.
784   Skamarock, W. C., Klemp, J. B., Dudhia, J., Gill, D. O., Barker, D. M., Wang, W., and Powers, J.
785   G.: A Description of the Advanced Research WRF Version 2, NCAR Technical Note, available
786   at: http://www2.mmm.ucar.edu/wrf/users/docs/arw_v2_070111.pdf   (last   access: 12
787   September 2018), 2005.
788   Sofiev, M., Vankevich, R., Lanne, M., Koskinen, J., and Kukkonen, J.: On integration of a Fire
789   Assimilation System and a chemical transport model for near-real-time monitoring of the
790   impact of wild-land fires on atmospheric composition and air quality, Modelling, Monitoring
791   and Management of Forest Fires, WIT Trans. Ecol. Envir., 119, 343–351, 2008a.
792   Sofiev, M., Lanne, M., Vankevich, R., Prank, M., Karppinen, A., and Kukkonen, J.: Impact of
793   wild-land fires on European air quality in 2006–2008, Modelling, Monitoring and Management
794   of Forest Fires, WIT Trans. Ecol. Envir., 119, 353–361, 2008b.
795   Sogacheva, L., Hamed, A., Facchini, M. C., Kulmala, M., and Laaksonen, A.: Relation of air mass
796   history to nucleation events in Po Valley, Italy, using back trajectories analysis, Atmos. Chem.
797   Phys., 7, 839–853, https://doi.org/10.5194/acp-7-839-2007, 2007.
798   Spracklen, D. V., Pringle, K. J., Carslaw, K. S., Chipperfield, M. P., and Mann, G. W.: A global
799   off-line model of size- resolved aerosol microphysics: I. Model development and pre- diction
800   of aerosol properties, Atmos. Chem. Phys., 5, 2227– 2252, doi:10.5194/acp-5-2227-2005,
801   2005.

802   Stanier, C. O., Pathak, R. K. and Pandis, S. N.: Measurements of the volatility of aerosols from a-
803   pinene ozonolysis, Environ. Sci. Technol., 41, 2756–2763, 2007.

804   Vehkamäki, H., Kulmala, M., Napari, I., Lehtinen, K. E. J., Timm- reck, C., Noppel, M., and
805   Laaksonen, A.: An improved parameterization for sulfuric acid-water nucleation rates for
806   tropospheric and stratospheric conditions, J. Geophys. Res., 107, 4622–4632, 2002.

807   Visschedijk, A. J. H., Zandveld, P., and Denier van der Gon, H. A. C.: TNO Report 2007 A-
808   R0233/B: A high resolution gridded European emission database for the EU integrated project
809   GEMS, Organization for Applied Scientific Research, the Netherlands, 2007.

810   Volkamer, R., Jimenez, J. L., San Martini, F., et al.: Secondary organic aerosol formation from
811   anthropogenic air pollution: Rapid and higher than expected, Geophys. Res. Lett., 33, L17811,
812   doi:10.1029/2006GL026899, 2006.

813   Wang, M. and Penner, J. E.: Aerosol indirect forcing in a global model with particle nucleation,
814   Atmos. Chem. Phys., 9, 239–260, https://doi.org/10.5194/acp-9-239-2009, 2009.

815   Yli-Juuti, T., Mohr, C., and Riipinen, I. Open questions on atmospheric nanoparticle
816   growth. Commun. Chem. 3, 106, https://doi.org/10.1038/s42004-020-00339-4, 2020.

817   Yu, F. and Luo, G.: Simulation of particle size distribution with a global aerosol model:
818   contribution of nucleation to aerosol and CCN number concentrations, Atmos. Chem. Phys.,
819   9, 7691– 7710, doi:10.5194/acp-9-7691-2009, 2009.

820   Zhang, Q., Jimenez, J. L., Canagaratna, M. R., Allan, J. D., Coe, H., Ulbrich, I., Alfarra, M. R.,
821   Takami, A., Middlebrook, A. M., Sun, Y. L., Dzepina, K., Dunlea, E., Docherty, K., DeCarlo,
822   P. F., Salcedo, D., Onasch, T., Jayne, J. T., Miyoshi, T., Shimono, A., Hatakeyama, S.,
823   Takegawa, N., Kondo, Y., Schneider, J., Drewnick, F., Borrmann, S., Weimer, S., Demerjian,
824   K., Williams, P., Bower, K., Bahreini, R., Cottrell, L., Griffin, R. J., Rautiainen, J., Sun, J. Y.,
825   Zhang, Y. M., and Worsnop, D. R.: Ubiquity and dominance of oxygenated species in organic
826   aerosols in anthropogenically-influenced Northern Hemisphere midlatitudes, Geophys. Res.
827   Lett., 34, L13801, doi:10.1029/2007GL029979, 2007.

828

829

830 **Table 1:** Prediction skill metrics of PMCAMx-UF against daily ground measurements of particle
831 number concentration above 10 nm (N_{10}) during 5 June – 8 July 2012.

832

Station	Mean Observed (cm^{-3})	Mean Predicted (cm^{-3})		NMB (%)		NME(%)	
		Base case	Without ELVOCs	Base case	Without ELVOCs	Base case	Without ELVOCs
N_{10}							
ANB	8057	6617	6585	-18	-18	39	39
ASP	2130	5233	5202	146	144	144	144
BRK	1878	3144	3053	67	63	86	86
CBW	13101	9913	9817	-24	-25	31	31
DSN	10591	6508	6504	-39	-39	41	41
DSW	7706	6111	6091	-21	-21	40	40
FNK	3962	5466	5466	38	38	40	40
GDN	5712	6652	6731	16	18	32	32
HOH	3438	3070	2906	-11	-15	38	38
HYY	2207	2536	2265	15	3	31	31
ISP	6232	6449	6203	3	0	43	43
KPU	5269	5855	5937	11	13	43	43
KST	3596	4881	4834	36	34	46	46
MLP	5583	6034	6003	8	8	42	42
MNT	6455	8364	8273	30	28	45	45
PRG	7272	7281	7273	0	0	44	44
USM	15171	8335	8413	-45	-45	52	52
VAV	3250	8291	8283	155	155	155	155
VRR	1107	1491	1190	35	7	69	57
VSM	2903	7281	7011	151	141	151	141
WLD	4956	7903	7783	59	57	66	64
ZUG	1237	2405	2287	94	85	111	103
NEO	2864	5085	5039	78	76	79	78
PAT	4705	5151	5148	9	9	45	44
SPC	8301	7198	7180	-13	-14	35	35
THE	3894	8577	8530	120	119	120	119
ALL	**4820**	**5957**	**5889**	**23**	**22**	**63**	**63**

833

834

835

836

Table 2: Prediction skill metrics of PMCAMx-UF against daily ground measurements of particle
number concentration above 100 nm (N_{100}) during 5 June – 8 July 2012.

839

Station	Mean Observed (cm⁻³)	Mean Predicted (cm⁻³)		NMB (%)		NME(%)	
		Base case	Without ELVOCs	Base case	Without ELVOCs	Base case	Without ELVOCs
N_{100}							
ANB	1518	939	934	-38	-38	47	47
ASP	552	789	694	43	26	61	51
BRK	607	419	397	-31	-35	65	62
CBW	1627	1550	1441	-5	-11	18	16
DSN	1976	1178	1052	-40	-47	44	49
DSW	1426	1156	1050	-19	-26	35	37
FNK	1760	2383	2330	35	32	39	36
GDN	2492	2797	2826	12	13	34	33
HOH	1011	697	656	-31	-35	37	40
HYY	677	579	445	-14	-34	26	38
ISP	1775	1334	1283	-25	-28	37	38
KPU	1543	1898	1861	23	21	29	28
KST	1123	1138	1061	1	-6	26	21
MLP	1214	1111	977	-9	-20	30	33
MNT	1492	1871	1799	25	21	49	50
PRG	1177	1256	1167	7	-1	26	25
USM	1657	1091	985	-34	-41	40	44
VAV	766	942	899	23	17	48	48
VRR	324	166	90	-49	-72	63	77
VSM	704	747	643	6	-9	34	34
WLD	1116	1063	955	-5	-14	20	23
ZUG	555	555	546	0	-2	44	44
NEO	1489	2041	1971	37	32	45	42
PAT	1747	1765	1766	1	1	21	23
SPC	1702	2051	1978	21	16	36	36
THE	1387	2420	2384	74	72	78	76
ALL	**1198**	**1326**	**1258**	**10**	**5**	**45**	**45**

840

841

842

843

844   **Table 3:** Predicted (PMCAMx-UF) and observed (AMS) average PM$_1$ concentrations of sulfate,

845   ammonium and nitrate in different locations for base case simulation.

Station	Sulfate		Ammonium		Nitrate	
	Predicted	Observed	Predicted	Observed	Predicted	Observed
	(μg m^{-3})	(μg m^{-3})	(μg m^{-3})	(μg m^{-3})	(μg m^{-3})	(μg m^{-3})
FIN	4.44	3.50	1.82	1.06	1.00	0.07
PAT	2.83	3.35	1.34	0.95	0.84	0.10
BOL	2.11	2.79	1.08	1.00	0.90	0.60
SPC	2.31	1.81	1.16	0.88	0.99	1.20
ALL	2.99	2.82	1.37	0.97	0.94	0.52

846

847

848   **Table 4:** Prediction skill metrics of PMCAMx-UF base case simulation against daily PM$_1$ OA

849   measurements.

Station	Mean Predicted (μg m^{-3})	Mean Observed (μg m^{-3})	NMB (%)	NME (%)	Factor of 2 (%)
FIN	3.19	2.12	50	51	83
PAT	2.75	3.80	-28	28	95
BOL	4.62	5.68	-19	33	74
SPC	4.74	3.98	19	44	77
ALL	3.87	3.79	2	38	82

850

851

852 **Table 5:** Prediction skill metrics of PMCAMx-UF against daily PM$_{2.5}$ OA measurements.

Name	Station	Country	Mean Observed ($\mu g\ m^{-3}$)	Mean Predicted ($\mu g\ m^{-3}$)	NMB (%)	NME (%)	Factor of 2 (%)
CH02	Payerne	Switzerland	2.54	2.98	17	73	72
DE44	Melpitz	Germany	2.52	4.42	76	88	66
ES1778	Montseny	Spain	4.52	6.28	39	89	59
IT04	Ispra	Italy	5.13	4.41	-14	46	71
PL05	Diabla Gora	Poland	3.64	4.22	16	43	84
SI08	Iskrba	Slovenia	5.98	5.07	-15	33	80
ALL			**4.06**	**4.56**	**20**	**62**	**72**

853

854
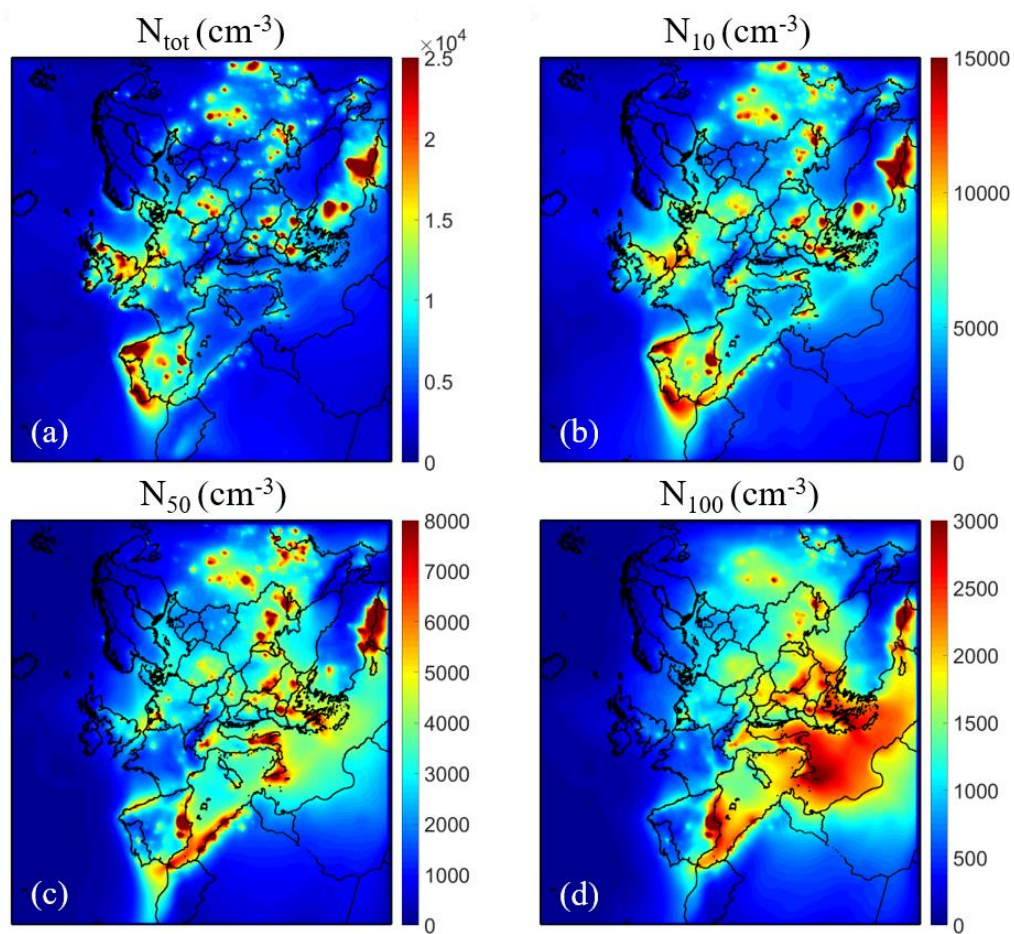
Figure 1: Average ground level number concentrations (in cm^{-3}) for the base case simulation during 5 June – 8 July 2012 for: (a) all particles (N_{tot}); and particles above (b) 10 nm (N_{10}); (c) 50 nm (N_{50}); and (d) 100 nm (N_{100}). Different scales are used.
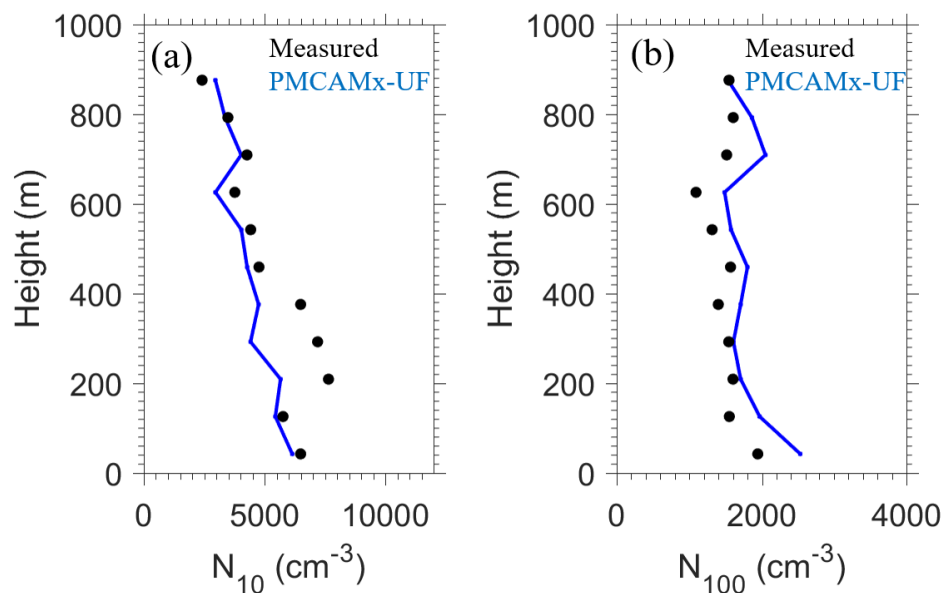
Figure 2: Comparison of predicted PMCAMx-UF (blue line) vs. observed (black dots) vertical
profiles of averaged particle number concentrations for (a) N_{10} and (b) N_{100} of 25 flights over the
Po Valley during the PEGASOS campaign.

863

864
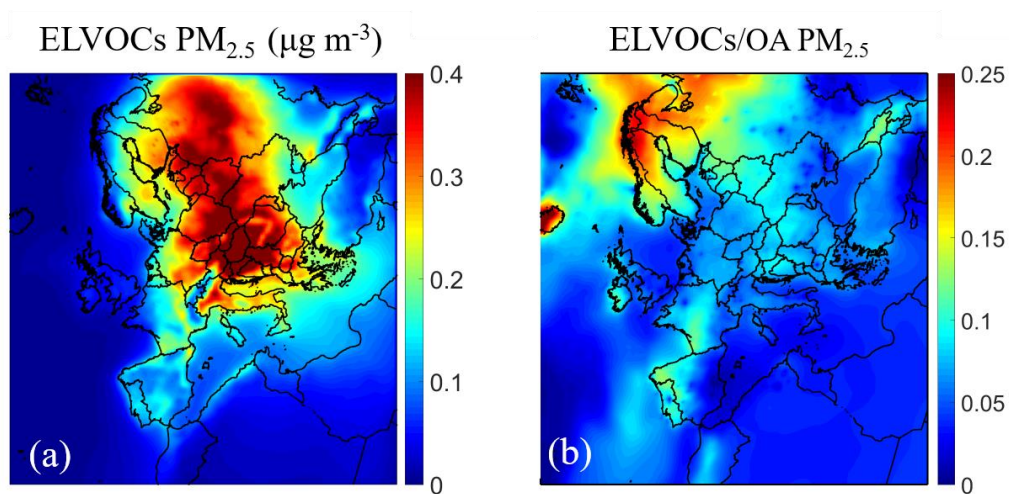
Figure 3: Average ground level (a) PM$_{2.5}$ ELVOCs mass concentration (in μg m^{-3}) and (b) the
ratio of the PM$_{2.5}$ mass of ELVOCs to OA during the simulation. Different scales are used.

867

868

869
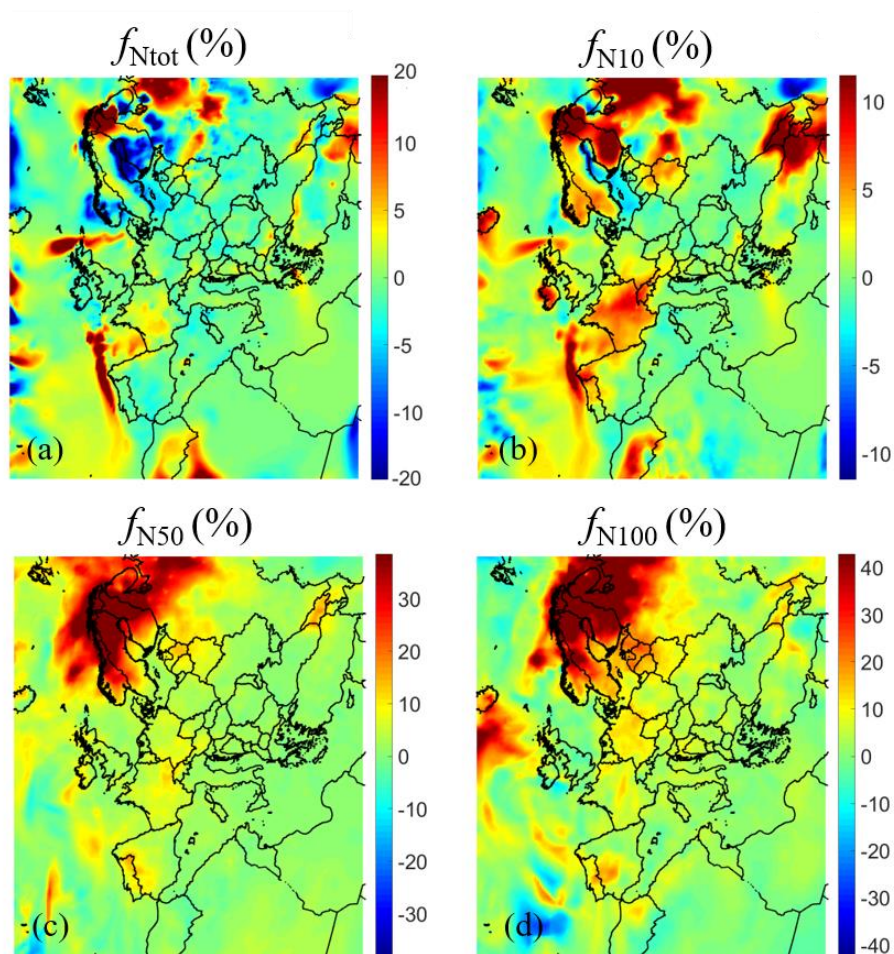
Figure 4: Average ground level fractional increase (f_{Nx}) of number concentration due to the
condensation of ELVOCs for: (a) all particles (f_{Ntot}); (b) particles above 10 nm (f_{N10}); (c) above 50
nm (f_{N50}); and (d) above 100 nm (f_{N100}). Different scales are used.

873

874

875

876

877

878
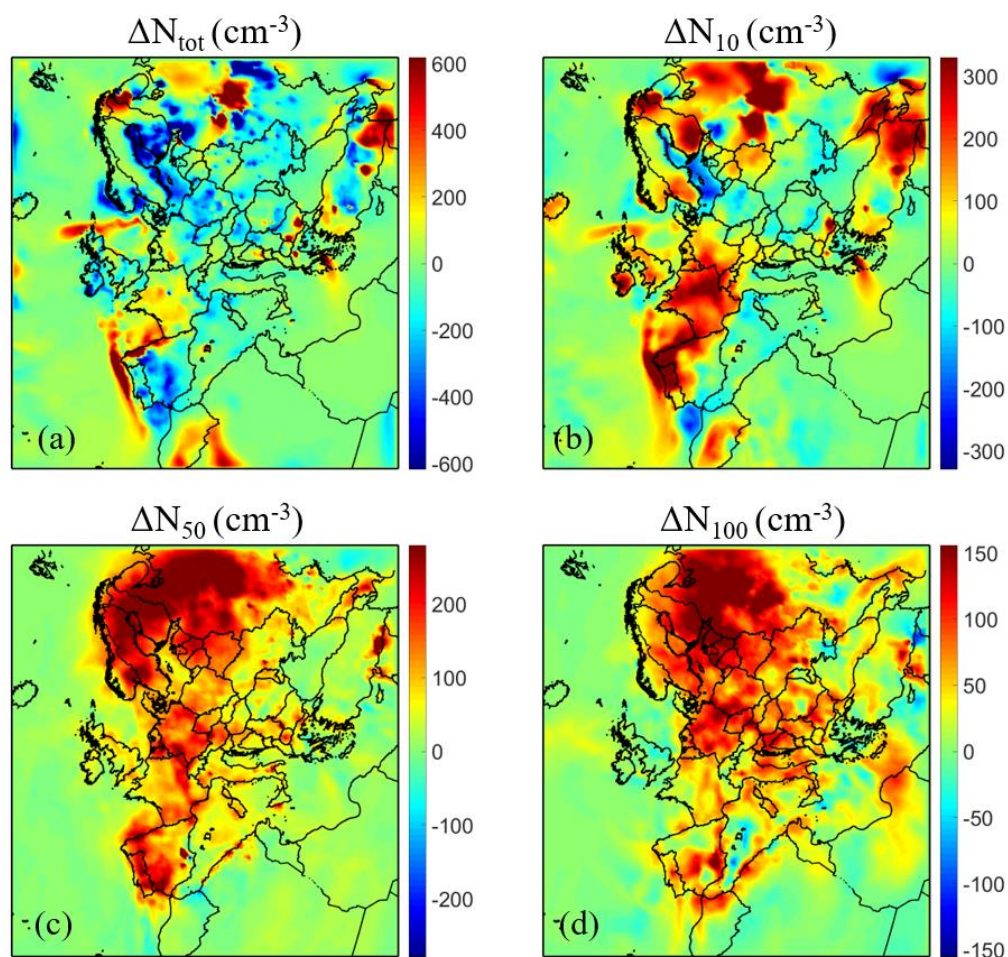
Figure 5: Average ground level increase of number concentration (in cm^{-3}) due to the condensation of ELVOCs for: (a) all particles (ΔN_{tot}); particles above (b) 10 nm (ΔN_{10}); (c) 50 nm (ΔN_{50}); and (d) 100 nm (ΔN_{100}). Different scales are used.

879
880
881
882
883
884
885
886
887

888

Figure 6: Ground level average (a) increase of PM$_{2.5}$ mass concentration of organics aerosol (in μg m^{-3}) and (b) fractional increase of PM$_{2.5}$ mass concentration of organics aerosol (%) due to the addition of IVOCs emissions of semi-volatility organic aging, predicted during 5 June – 8 July. Different scales are used.

893

894

895

896

897

898

899

900

901

902

903

904
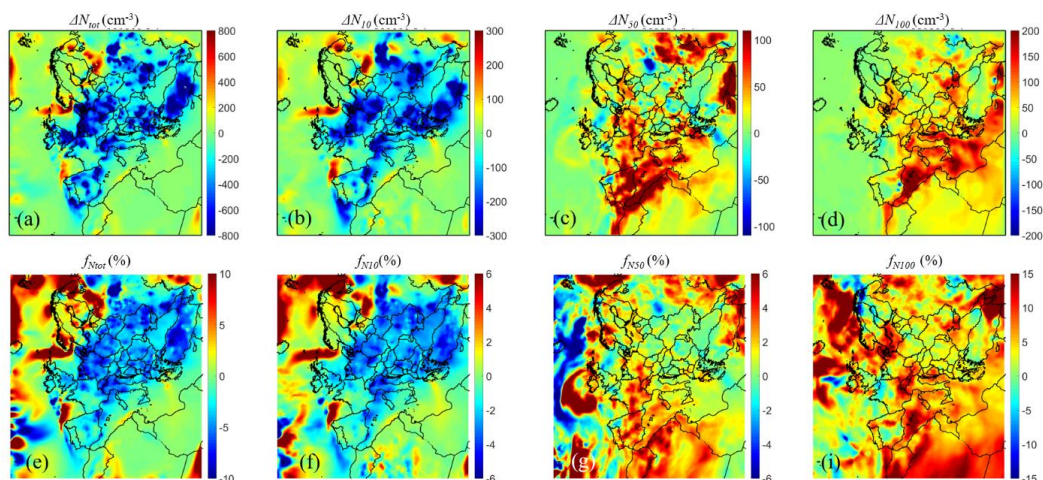
Figure 7: Ground level increase of number concentration (in cm^{-3}) (a-d) and fractional increase (f_{Nx}) of number concentration (e-i) due to the addition of IVOCs emissions and aging reactions, predicted during 5 June – 8 July 2012 for: (a, e) all particles (N_{tot}); and particles above (b, f) 10 nm (N_{10}); (c, g) 50 nm (N_{50}); and (d, i) 100 nm (N_{100}). Different scales are used.

912
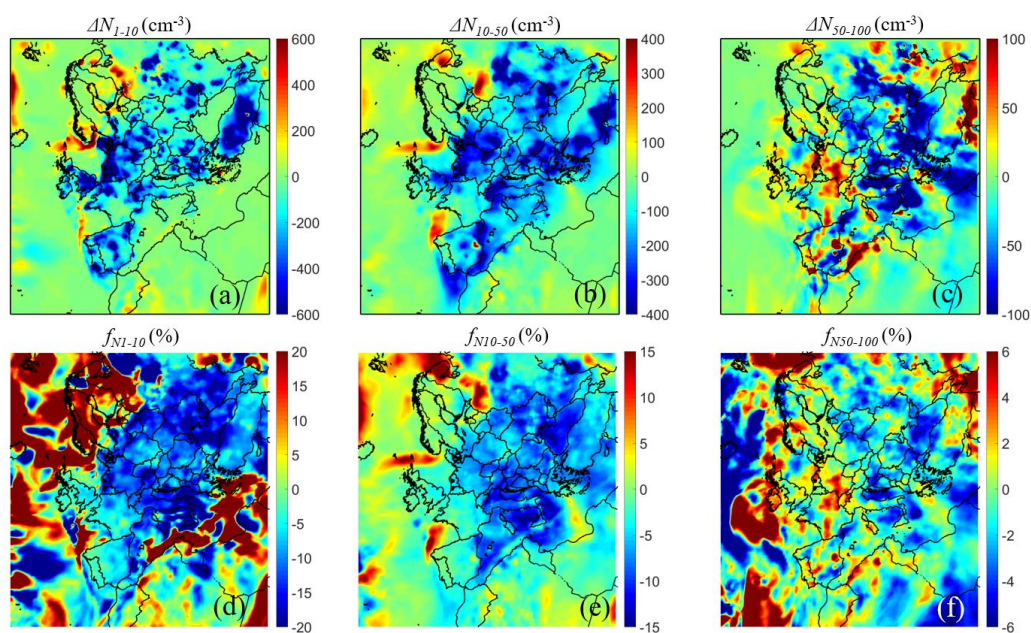
Figure 8: Ground level average increase of number concentration (in cm^{-3}) (a-b-c) and fractional
increase (f_{Nx}) of number concentration (d-e-f) due to the addition of IVOCs emissions predicted
during 5 June – 8 July 2012 for: (a, d) particles between 0.8 nm and 10 nm (N_{1-10}); (b, e) particles
between 10 nm and 50 nm (N_{10-50}) and (c, f) particles between 50 nm and 100 nm (N_{50-100}).
Different scales are used.